Miner Deposita (2009) 44:371–387
DOI 10.1007/s00126-008-0210-6

ARTICLE

U–Pb, Re–Os, and $^{40}Ar/^{39}Ar$ geochronology of the Nambija Au-skarn and Pangui porphyry Cu deposits, Ecuador: implications for the Jurassic metallogenic belt of the Northern Andes

Massimo Chiaradia · Jean Vallance · Lluis Fontboté · Holly Stein · Urs Schaltegger · Joshua Coder · Jeremy Richards · Mike Villeneuve · Ian Gendall

Received: 2 May 2008 / Accepted: 14 September 2008 / Published online: 8 October 2008

Abstract New U–Pb, Re–Os, and $^{40}Ar/^{39}Ar$ dates are presented for magmatic and hydrothermal mineral phases in skarn- and porphyry-related ores from the Nambija and Pangui districts of the Subandean zone, southeastern Ecuador. Nambija has been one of the main gold-producing centers of Ecuador since the 1980s due to exceptionally high-grade ores (average 15 g/t, but frequently up to 300 g/t Au). Pangui is a recently discovered porphyry Cu–Mo district. The geology of the Subandean zone in southeastern Ecuador is dominated by the I-type, subduction-related, Jurassic Zamora batholith, which intrudes Triassic volcanosedimentary rocks. The Zamora batholith is in turn cut by porphyritic stocks, which are commonly associated with skarn formation and/or porphyry-style mineralization. High precision U–Pb and Re–Os ages for porphyritic stocks (U–Pb, zircon), associated prograde skarn (U–Pb, hydrothermal titanite), and retrograde stage skarn (Re–Os, molybdenite from veins postdating gold deposition) of the Nambija district are all indistinguishable from each other within error (145 Ma) and indicate a Late Jurassic age for the gold mineralization. Previously, gold mineralization at Nambija was considered to be Early Tertiary based on K–Ar ages

Editorial handling: B. Lehmann

Electronic supplementary material The online version of this article (doi:10.1007/s00126-008-0210-6) contains supplementary material, which is available to authorized users.

M. Chiaradia (✉) · J. Vallance · L. Fontboté · U. Schaltegger
Section des Sciences de la Terre, University of Geneva,
Rue des Maraîchers 13,
1205 Geneva, Switzerland
e-mail: Massimo.Chiaradia@terre.unige.ch

J. Vallance
Pan American Silver Peru SAC,
Av. La Floresta 497, Of. 301, Chacarilla del Estanque, San Borja,
Lima, Peru

H. Stein
AIRIE Program, Department of Geosciences,
Colorado State University,
Fort Collins, CO 80523-1482, USA

H. Stein
Geological Survey of Norway,
Leiv Eirikssons vei 39,
7491 Trondheim, Norway

J. Coder · J. Richards
Department Earth and Atmospheric Sciences,
University of Alberta,
Edmonton, Alberta, Canada T6G 2E3

M. Villeneuve
Geological Survey of Canada—Ottawa,
601 Booth Street,
Ottawa, Ontario K1A 0E8, Canada

I. Gendall
Chapleau Resources Ltd.,
Suite #104, 135-10th Avenue South,
Cranbrook, BC V1C 2NI, Canada

obtained on various hydrothermal minerals. The new Jurassic age for the Nambija district is slightly younger than the $^{40}Ar/^{39}Ar$ and Re–Os ages for magmatic–hydrothermal minerals from the Pangui district, which range between 157 and 152 Ma. Mineralization at Nambija and Pangui is associated with porphyritic stocks that represent the last known episodes of a long-lived Jurassic arc magmatism (~190 to 145 Ma). A Jurassic age for mineralization at Nambija and Pangui suggests that the Northern Andean Jurassic metallogenic belt, which starts in Colombia at 3° N, extends down to 5° S in Ecuador. It also adds a new mineralization style (Au-skarn) to the metal endowment of this belt.

Keywords U–Pb · Re–Os · Ar–Ar · Geochronology · Ecuador · Nambija · Pangui · Skarn · Porphyry Cu · Gold

Introduction

Mineralization in the porphyry environment is associated with subduction-related calc-alkaline magmatism and is characterized by the spatial coexistence of different deposit types (e.g., porphyry Cu, skarn, epithermal). In this environment, accurate and precise geochronology is essential to elucidate how the different styles of mineralization relate to each other, to the magmatic activity, and to the geodynamic context. This kind of information allows the elaboration of metallogenic models that are instrumental to mineral exploration at the regional scale.

Dating ore deposits in the porphyry environment can either be done directly on appropriate ore minerals where available (e.g., Re–Os dating of molybdenite) or indirectly on (1) alteration mineral phases considered to be coeval to the ore event or (2) primary igneous mineral phases from the magmatic body associated with the mineralization. Ideally, the combined dating of ore, alteration, and magmatic stage minerals obtained through different radiometric methods (e.g., U–Pb, Re–Os, $^{40}Ar/^{39}Ar$) provides the tools for a more robust geochronological evaluation of the mineralizing event and additional information on the temporal development of ore formation (see Maksaev et al. 2004; Deckart et al. 2005).

The porphyry-related, gold skarn district of Nambija has been one of the main gold producers of Ecuador with an estimated 62 t of gold extracted mostly by artisanal methods since the 1980s. Previous K–Ar dating (Prodeminca 2000) has yielded Late Jurassic to Early Cretaceous dates for skarn formation and Cu–Mo porphyry mineralization and Paleocene to Eocene dates for gold deposition, resulting in interpretation of the gold mineralization as a Tertiary epithermal event superimposed onto the Jurassic "barren" skarn. However, data reported by Markowski (2003), Vallance et al. (2003), Fontboté et al. (2004), and Markowski et al. (2006) are inconsistent with the large temporal decoupling (Jurassic to Tertiary) of porphyry mineralization, skarn formation, and gold deposition proposed by Prodeminca (2000) and suggest that the K–Ar ages are strongly disturbed by subsequent thermal events.

In this study, we present new U–Pb geochronological data on magmatic zircon and hydrothermal titanite and Re–Os ages on hydrothermal molybdenite from the Nambija skarns to constrain the magmatic–hydrothermal evolution of the mineralization using robust geochronometers. We also compare these Re–Os and U–Pb ages for Nambija with new Re–Os and $^{40}Ar/^{39}Ar$ ages for magmatic and hydrothermal phases from porphyry mineralization in the Pangui district situated 70 km north of Nambija and with available ages for porphyry Cu deposits from Colombia. We finally discuss the Nambija district mineralization in the broader metallogenic and geodynamic context of the Northern Andes.

Geological setting

The Nambija gold skarn deposits and the porphyry Cu–(Mo–Au) deposits of the Pangui district (Litherland et al. 1994; Paladines and Rosero 1996; Gendall et al. 2000; Prodeminca 2000) are located in the Cordillera del Cóndor in the Subandean zone of southeastern Ecuador (Fig. 1). They are part of a metallogenic belt that extends in a northerly direction for almost 100 km, which also contains low-sulfidation epithermal Au–Ag deposits of poorly defined age (e.g., Chinapintza: K–Ar age on biotite of 96±10 Ma; Prodeminca 2000) or inferred to be Jurassic (Fruta del Norte; Stewart and Leary 2007).

The geology of this part of the Ecuadorian Andes is dominated by Jurassic (K–Ar ages from 190 to 150 Ma and a Rb–Sr isochron age of 187±2 Ma; Litherland et al. 1994) calc-alkaline I-type, granodioritic to tonalitic intrusions of the Zamora batholith (Litherland et al. 1994; Quispesivana 1996). This batholith extends for about 200 km along a NNE trend between latitudes 5° S and 3° S (Fig. 1). Together with other intrusions to the north (Abitagua, 162± 1 Ma, Rb–Sr whole rock isochron; Azafran, 142.7±1 Ma, U–Pb on zircon; Litherland et al. 1994), the Zamora batholith is considered to be the plutonic expression of a Jurassic subduction-related continental magmatic arc established on the western margin of the Amazon craton (Litherland et al. 1994). Volcanic rocks of the Misahualli unit dated at 172.3±2.1 Ma ($^{40}Ar/^{39}Ar$; Romeuf et al. 1995) and 162±2 Ma ($^{40}Ar/^{39}Ar$; Spikings et al. 2001), which overlie and/or are associated with the batholith (Fig. 1), are considered to be the extrusive expression of the Jurassic continental arc. Continental to marine sedimentary and

volcanosedimentary rocks of the Triassic Piuntza unit (Aspden and Litherland 1992; Litherland et al. 1994; Pratt et al. 2005) occur locally as flat, eroded roof pendants at the top of the Zamora batholith (Litherland et al. 1994).

A protracted period of uplift led to a ≥20-My hiatus in sedimentation (Barragan et al. 2005) and unroofing of the Zamora batholith until the unconformable deposition, on top of the Zamora batholith and Misahualli unit, of the marine Hollín Formation (Aptian–Albian; Jaillard et al. 2000; Pratt et al. 2005). It is not clear why arc magmatism stopped at the end of the Jurassic and never resumed in the Subandean zone. According to Litherland et al. (1994), Jurassic subduction beneath the Amazon craton was terminated in Late Jurassic–Early Cretaceous times by accretion of the Alao island arc and the continental Chaucha terrane. This accretionary event (known as Peltetec: Aspden and Litherland 1992) could have also caused uplift of the Eastern Cordillera and Subandean zone. Slab roll-back after collision of the above terranes with the western margin of the Amazon craton would have been responsible for Cretaceous back-arc alkaline magmatism in the Oriente basin, east of the Subandean zone (Barragan et al. 2005). The wide range of imprecise K–Ar dates previously published for the Zamora batholith (~150 to ~100 Ma) is considered to reflect thermal disturbance caused by the Peltetec accretionary event (Litherland et al. 1994). However, Pratt et al. (2005) have questioned this model because of the lack of geological and structural evidence for accretionary events in the Eastern Cordillera of Ecuador. In this case, other processes could be responsible for the Cretaceous hiatus in magmatic arc activity (e.g., slow, oblique, or low-angle subduction; Kennan and Pindell 2003; change in subduction direction from southward to northeastward; Aspden et al. 1987; Jaillard et al. 1990, 2000).

Subsequently, the Eastern Cordillera and the Subandean zone were uplifted during the Late Cretaceous to Paleocene in response to the accretion of the Pallatanga oceanic terrane (Fig. 1; Spikings et al. 2000; Kerr et al. 2002; Hughes and Pilatasig 2002; Jaillard et al. 2005; Pratt et al. 2005; Vallejo et al. 2006).

Mineralization styles

Nambija district

The main mineralization style in the Nambija district consists of skarn-associated Au-bearing veins with minor porphyry Cu–Mo mineralization (Fig. 1: Cumay, David, Tumi prospects; Prodeminca 2000). During the past decades, the Nambija gold skarn deposits have been among the main sources of gold in Ecuador, exploited mostly by artisanal methods. The deposits, which had estimated resources of 11.5 Moz Au in 1990 (Mining Magazine as reported by Prodeminca 2000) with a past production of 62 t Au in the 1980s (Gemuts et al. 1992), contain exceptionally high grades (average 15 g/t Au, but frequently up to 300 g/t Au; Prodeminca 2000).

The gold skarn deposits occur along a 20-km long north–south corridor within an elongated lens of the Triassic Piuntza unit (Fig. 1), which constitutes a roof pendant within the Zamora batholith (Markowski 2003; Vallance et al. 2003; Fontboté et al. 2004; Markowski et al. 2006). Several individual discontinuous skarn orebodies occur from north to south: Fortuna, Cambana, Campanillas, Nambija, Guaysimi, and Sultana del Cóndor (Fig. 1). The deposits are spatially associated with granodiorite and porphyritic quartz–diorite intrusions cutting the Zamora batholith and the Piuntza unit along structurally controlled intersections between N–S lineaments and NW-trending faults (Fig. 1; see also Richards 2000). The porphyritic intrusions show an inner potassic alteration zone grading into an outer endoskarn zone and exoskarn in the volcanosedimentary Piuntza unit. Some of the porphyritic intrusions contain porphyry-style Cu–Mo mineralization spatially associated with the skarn (e.g., the David Cu–Mo porphyry and Guaysimi skarn; Fig. 1).

Skarns consist of a dominant prograde stage (expressed mostly as exoskarn overprinting the Piuntza volcanosedimentary lithologies, but also as endoskarn within the porphyritic stocks) with a weak retrograde overprint. The prograde exoskarn is dominated by a typical oxidized skarn-type mineralogy consisting of massive brown andraditic garnet (mean Ad_{38}) with subordinate pyroxene and epidote (Fontboté et al. 2004). More andraditic garnets occur in later blue–green skarns and yellow–brown clusters/bands (with means of Ad_{45} and Ad_{84}, respectively; Fontboté et al. 2004).

The weakly developed retrograde stage consists essentially of vugs and veins with quartz, K-feldspar, calcite, chlorite, hematite±plagioclase±muscovite, and minor amounts of sulfide minerals (pyrite, sphalerite). Gold deposition occurred during this weakly developed retrograde stage under oxidizing conditions (Markowski 2003; Vallance et al. 2003; Fontboté et al. 2004; Markowski et al. 2006), mainly in structurally controlled, elongated vugs trending N10°–60°E (Fig. 2a, c, d), and up to several-centimeters-wide quartz-bearing sulfide-poor veins (type I and type II veins of Fontboté et al. 2004). Later type III, molybdenite-bearing, sulfide-rich veins do not contain gold.

Fluid inclusion and stable isotope studies (Vallance et al., unpublished data) suggest that magmatic fluids are responsible for the prograde stage and the main part of the retrograde skarn stages, including gold deposition.

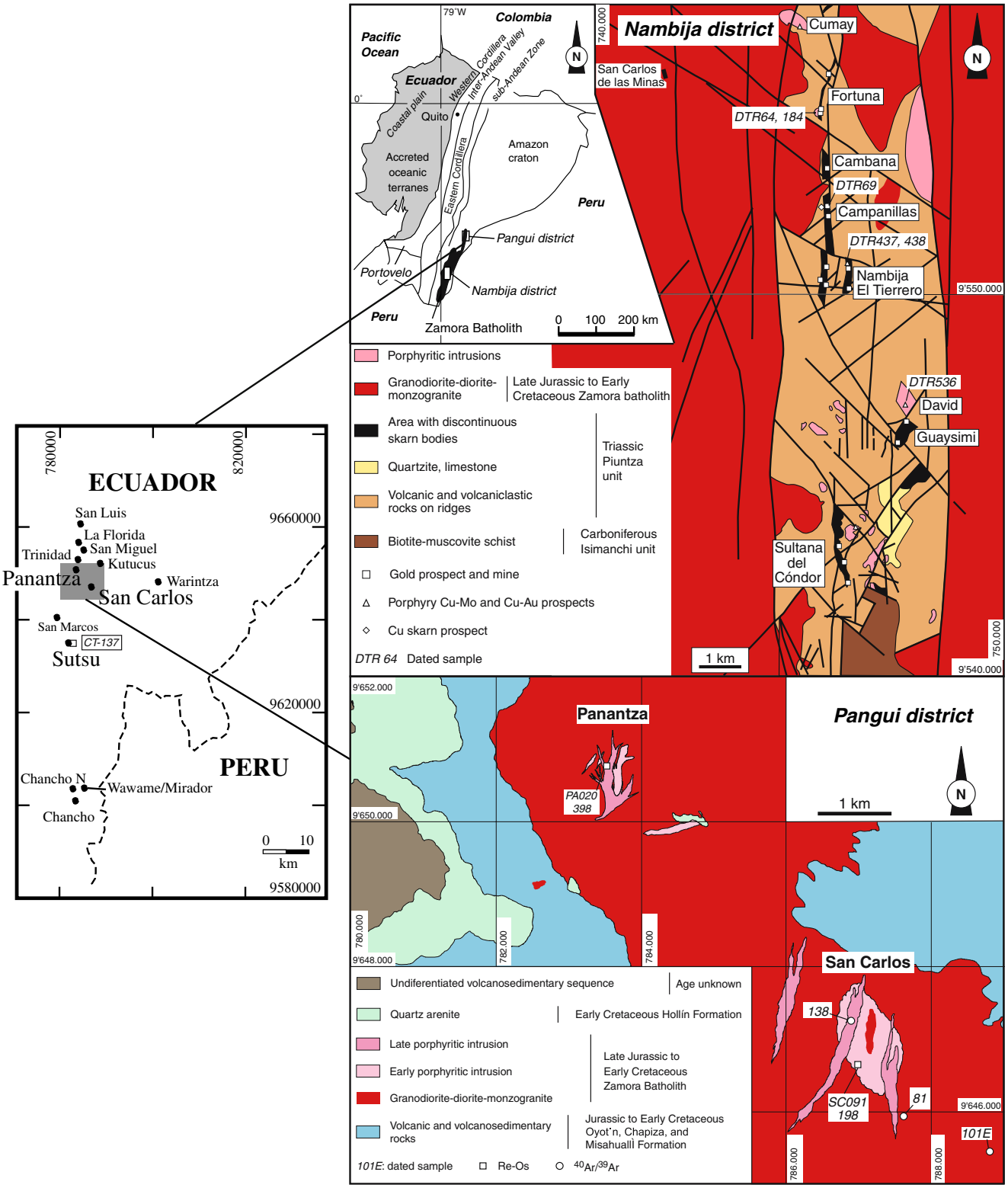

Fig. 1 Geological maps of the Nambija (*top right*) and Pangui (*bottom right*) districts with location of the dated samples. *Upper left inset* geotectonic map of Ecuador showing the location of the Pangui and Nambija districts. *Middle left inset* map of porphyry Cu and skarn prospects in the Pangui district (modified after Gendall et al. 2000). The prospects investigated in this study (San Carlos, Panantza, and Sustsu) are indicated by *larger fonts*. The *shaded area* corresponds to the area of the geological map of the Pangui district (*bottom right*)

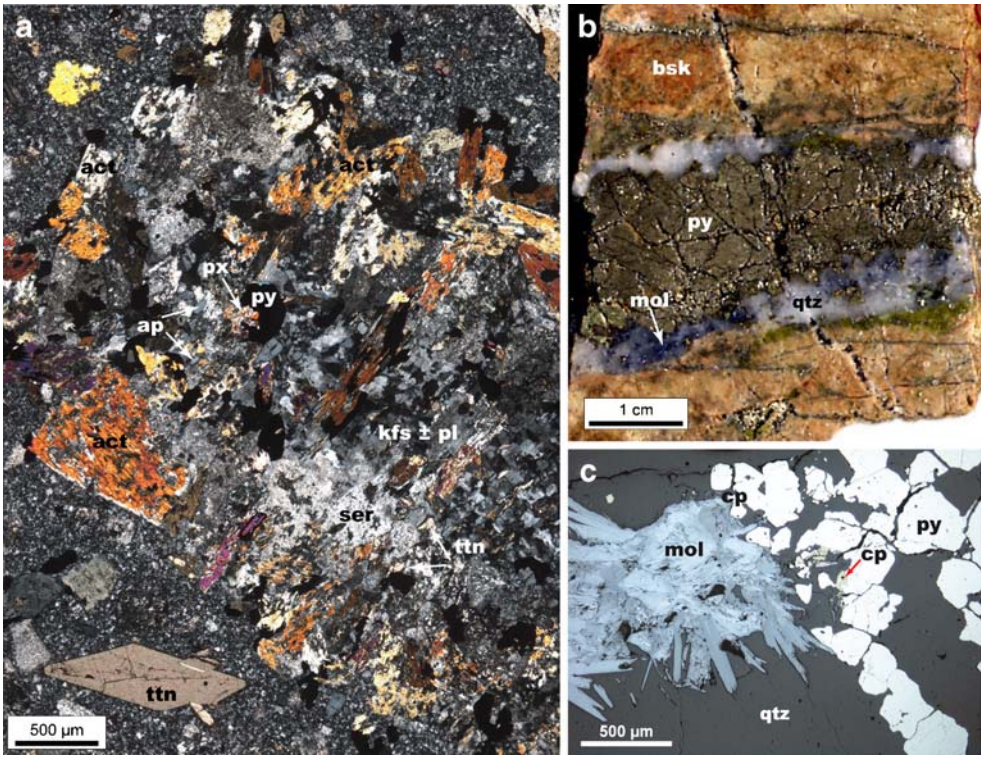

Fig. 2 **a** Photomicrograph of endoskarn assemblage with titanite (*ttn*) (transmitted light, crossed nicols); **b** molybdenite (*mol*) in a sulfide-rich type III vein cutting through brown skarn (*bsk*); **c** photomicrograph of molybdenite in sulfide-rich type III vein (reflected light). Other abbreviations: *act* actinolite, *ap* apatite, *cp* chalcopyrite, *kfs* K-feldspar, *pl* plagioclase, *px* pyroxene, *py* pyrite, *qtz* quartz, *ser* sericite

Postgold, sulfide-rich veins (type III) correspond to late magmatic–hydrothermal fluid pulses mixed with meteoric water. Pressure estimates based on fluid inclusion studies (Vallance et al., unpublished data) indicate that the prograde skarn stage occurred at 100–120 MPa, equivalent to a depth of 3 to 4 km under lithostatic pressure conditions.

Pangui district

The Pangui area, located 70 km north of Nambija, is essentially a porphyry copper district (Fig. 1) comprising about ten known porphyry Cu–Mo prospects and one Cu-skarn prospect. The best studied of these deposits are the porphyry Cu–Mo prospects of San Carlos, Panantza, and Sutsu and the copper skarn prospect of Kutucus (Gendall et al. 2000; Prodeminca 2000; Coder 2001) (Fig. 1). The porphyry copper mineralization is hosted by small, composite granodiorite to porphyritic monzodiorite stocks, which intrude the Zamora batholith and the volcaniclastic rocks of the Misahualli unit (Fig. 1). The porphyries are affected by an early potassic alteration with associated hypogene chalcopyrite mineralization, which is locally overprinted by later intermediate argillic and sericitic alteration grading outwards into propylitic alteration. Quartz veinlets are poorly developed, and the chalcopyrite ore occurs mainly as disseminated grains and fracture coatings. Based on the dominance of pyrite-poor potassic alteration and subordinate sericitic alteration and brecciation, Gendall et al. (2000) suggested that a relatively deep (>3 km) level of the porphyries is exposed in the Pangui area.

The inferred hypogene resource for San Carlos has been evaluated at about 850 Mt at 0.5% Cu (Gendall et al. 2000). Most of the porphyries also contain 60 to 70 ppm (and up to 250 ppm) Mo and can be classified as Cu–Mo systems.

Previous age determinations

Several K–Ar dates for porphyritic intrusions and related mineralization in the Nambija and Pangui districts have been reported by Prodeminca (2000) and Gendall et al. (2000). These dates are mostly relatively imprecise (errors of several million years) and highly variable, suggesting that thermal overprinting has affected the K–Ar system in many of these deposits.

Nambija district

Hornblende from a porphyritic quartz–monzonite intrusion related to Cu–Mo porphyry mineralization at the Cumay prospect (Fig. 1) was dated at 141±5 Ma and was interpreted to date a synexoskarn or postexoskarn stage (Prodeminca 2000). Analysis of K-feldspar from a mineralized vein within the same intrusion yielded a younger date of 102±3 Ma.

Sericite was also dated from mineralized veins within the porphyritic granodiorite intrusion associated with Cu–Mo mineralization at the Nambija–El Tierrero prospect (Fig. 1; Prodeminca 2000). Dates of 100±3 and 116±4 Ma were

Table 1 Isotopic data of U–Pb age determinations on zircon and titanite of the Nambija district

	Mineral	Weight (mg)	Concentration			Th/U[a]	Atomic ratios							Ages			
			U (ppm)	Pb rad (ppm)	Pb com. (pg)		$^{206}Pb/^{204}Pb^{b}$	$^{207}Pb/^{206}Pb^{b,c,d}$	Error 2σ (%)	$^{207}Pb/^{235}U^{b,c}$	Error 2σ (%)	$^{206}Pb/^{238}U^{b,c,d}$	Error 2σ (%)	$^{206}Pb/^{238}U^{d}$	$^{207}Pb/^{235}U$	$^{207}Pb/^{206}Pb$	Corr coeff(rho)
DTR64—Mina Fortuna																	
1	tit	0.0836	40	1.73	56.00	3.60	105	0.04926	0.64	0.1545	1.00	0.02275	0.76	145.0	145.9	160.0	0.77
2	tit	0.0810	146	1.78	49.17	3.70	114	0.04944	0.69	0.1556	0.76	0.02282	0.24	145.5	146.8	168.9	0.44
3	tit	0.1323	30	0.62	62.60	2.85	117	0.04866	0.57	0.1660	0.70	0.02474	0.38	157.6	155.9	131.2	0.58
4	tit	0.0716	44	1.83	44.04	3.42	121	0.04874	0.55	0.1513	0.64	0.02251	0.26	143.5	143.1	135.2	0.52
5	zir	0.0013	369	8.51	0.53	0.40	1,383	0.04905	0.29	0.1543	0.41	0.02282	0.27	145.4	145.7	150.2	0.71
6	zir	0.0011	477	11.06	0.57	0.41	1,390	0.04893	0.20	0.1542	0.32	0.02286	0.23	145.7	145.6	144.6	0.78
7	zir	0.0009	533	12.68	3.35	0.52	227	0.04899	0.49	0.1540	0.57	0.02279	0.23	145.3	145.42	147.4	0.53
DTR184—Mina Fortuna																	
8	tit	0.0654	38	1.72	45.30	3.90	98	0.04932	0.98	0.1554	1.07	0.02285	0.30	145.6	146.6	162.9	0.43
9	tit	0.1097	40	1.71	69.06	3.53	110	0.04934	1.00	0.1551	1.07	0.02280	0.30	145.4	146.4	163.8	0.37
10	tit	0.0675	43	1.88	44.23	3.73	109	0.04904	0.52	0.1539	0.84	0.02276	0.64	145.1	145.4	150.0	0.79
11	zir	0.0027	413	9.77	0.42	0.48	4,053	0.04903	0.13	0.1545	0.28	0.02285	0.24	145.7	145.9	149.5	0.87
12	zir	0.0054	264	6.15	0.80	0.42	2,687	0.04902	0.11	0.1543	0.26	0.02283	0.23	145.5	145.7	148.8	0.90
13	zir	0.0020	341	7.91	2.30	0.41	459	0.04904	0.30	0.1546	0.40	0.02287	0.23	145.7	146.0	149.5	0.66
DTR69—Mina Campanillas																	
14	tit	0.1171	38	1.70	68.26	3.77	113	0.04926	0.58	0.1549	0.64	0.02280	0.24	145.4	146.2	160.3	0.43
15	tit	0.0927	39	1.80	56.40	3.98	112	0.04902	0.59	0.1540	0.67	0.02278	0.24	145.2	145.4	148.8	0.49
16	tit	0.0870	39	1.74	66.80	3.85	92	0.04888	0.68	0.1537	0.74	0.02281	0.23	145.4	145.2	141.9	0.41
17	zir	0.0038	183	4.41	1.36	0.55	771	0.04898	0.24	0.1541	0.34	0.02281	0.23	145.4	145.5	146.8	0.71
18	zir	0.0022	343	8.34	0.50	0.45	2,302	0.04901	0.16	0.1543	0.30	0.02283	0.25	145.5	145.7	148.2	0.84
19	zir	0.0030	391	9.34	1.07	0.53	321	0.04894	0.35	0.1538	0.45	0.02278	0.23	145.2	145.2	145.1	0.62
20	zir	0.0046	332	7.79	1.50	0.45	755	0.04896	0.19	0.1543	0.31	0.02285	0.23	145.7	145.7	146.0	0.78

tit titanite, *zir* zircon

[a] Calculated on the basis of radiogenic $^{208}Pb/^{206}Pb$ ratios, assuming concordance

[b] Corrected for fractionation and spike

[c] Corrected for fractionation, spike, blank and common lead (according to Stacey and Kramers 1975)

[d] Corrected for initial ^{230}Th disequilibrium, assuming a Th/U=4 in the source (for zircon analyses only)

obtained and are interpreted to be coeval with skarn formation. Potassium feldspar from the gold-bearing veins at Cambana and Guaysimi (Fig. 1) yielded much younger dates ranging from 48 to 65 Ma (Prodeminca 2000).

The large difference between the K–Ar dates obtained for skarn formation and gold deposition is inconsistent with the mineralization model of Fontboté et al. (2004) and Markowski et al. (2006) in which gold mineralization occurred during the retrograde skarn stage.

Pangui district

K–Ar age determinations on the San Carlos porphyritic granodiorite intrusion associated with copper mineralization yielded dates of 157±5 Ma (hornblende), 154±5 Ma (whole rock on sericitized porphyritic body), and 145±5 Ma on a sericite mineral separate (Gendall et al. 2000; Prodeminca 2000).

New geochronological studies

To determine more accurately the age of gold mineralization at Nambija, we have used robust geochronometers (Re–Os, U–Pb) to date minerals belonging to different stages of the magmatic–hydrothermal system. Similarly, in order to refine age determinations for magmatism and porphyry Cu–Mo mineralization in the Pangui district, we have sampled molybdenite and various magmatic and hydrothermal mineral phases for Re–Os and $^{40}Ar/^{39}Ar$ dating, respectively.

Details on the analytical methods used are provided in the Electronic Supplementary Material.

Nambija district samples

Magmatic zircon was dated using the U–Pb method to obtain an age for the porphyritic stocks likely responsible for skarn formation and porphyry Cu–Mo mineralization. Magmatic zircon was separated from two samples of the porphyritic quartz–diorite intrusion that crops out below the exoskarn in Fortuna (Fig. 1; samples DTR64 and DTR184) and from the porphyritic granodiorite intrusion spatially associated with the exoskarn in the abandoned Campanillas–Katy workings (Fig. 1; sample DTR69). Ten zircon grains were analyzed in total (three from sample DTR64, three from sample DTR184, and four from sample DTR69). The clearest, most transparent, inclusion-free, and elongated prismatic zircon crystals (rarely exceeding 50 μm in length) were hand-picked under a binocular microscope for analysis.

Hydrothermal titanite from the endoskarn was dated using the U–Pb method to obtain an age for prograde skarn formation; this date also provides a minimum age for crystallization of the associated intrusion and a maximum age for later gold deposition. Hydrothermal titanite was obtained from the endoskarn zones of Fortuna (samples DTR64 and DTR184) and Campanillas–Katy (sample DTR69). Euhedral and twinned titanite crystals up to 1.5 mm in size in Fortuna and up to 7 mm in size in Campanillas–Katy (Fig. 2a) occur where the endoskarn alteration (K-feldspar, actinolite, diopside, Na-rich plagioclase, titanite, quartz, apatite, and pyrite; Markowski et al. 2006) is more developed.

Hydrothermal molybdenite from the retrograde skarn stage that postdates gold deposition was dated using the Re–Os method, thereby providing a minimum age constraint for gold mineralization. Two molybdenite samples (DTR437 and DTR438) were collected at the exit of currently exploited galleries at Nambija–El Tierrero (Fig. 1). Molybdenite occurs

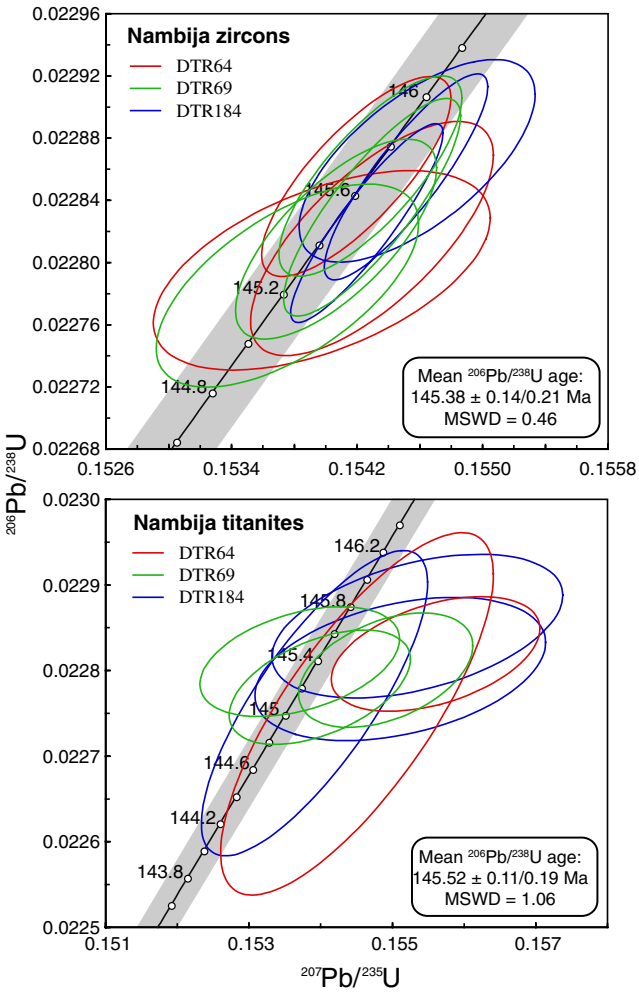

Fig. 3 Concordia diagrams of zircon (*top*) and titanite (*bottom*) samples from the Fortuna and Campanillas–Katy mines, Nambija district, with mean weighted $^{206}Pb/^{238}U$ ages and 2σ errors reported without and with decay constant uncertainties. The *shaded area* shows the 2σ uncertainty on the Concordia curve due to uncertainty of the decay constant. *Ellipses* represent 2σ uncertainties

in millimeter to several centimeter-thick type III veins together with gray–white quartz, pyrite, chalcopyrite, ±K-feldspar, and epidote, is very fine-grained (<500 μm), and is intergrown with chalcopyrite (Fig. 2c). The veins crosscut the brown garnet skarn (Fig. 2b).

Molybdenite from the David porphyry Cu–Mo deposit (Fig. 1) was also dated by Re–Os to compare the age of porphyry-style mineralization with the age of skarn-type mineralization in the Nambija district. Molybdenite was obtained from sample DTR536 collected in a valley 500 m northwest and 200 m below the level of the Guaysimi Banderas mine (Fig. 1). Molybdenite from this sample is fine-grained (<200 μm) and occurs in a stockwork of 1 to 7 mm-thick quartz veins with minor pyrite and chalcopyrite (<5%).

Pangui district samples

Molybdenite from the three main porphyry prospects in the Pangui district (San Carlos, Panantza, and Sutsu: Fig. 1) was sampled from drill cores (San Carlos: sample SC091198, 144.8 m; Panantza: sample PA020398, 249.5 m) and from a fresh surface sample at Sutsu (CT-137). These samples were all of quartz–molybdenite±chalcopyrite±pyrite B-type veins (sensu Gustafson and Hunt 1975) with sericite selvages.

$^{40}Ar/^{39}Ar$ analyses were carried out on mineral separates from three samples collected in the San Carlos prospect to obtain the ages of the Zamora batholith (hornblende: sample 101E), of a late porphyry dike (hornblende: sample 138), and of a hydrothermal breccia (muscovite: sample 81). For all three samples, two aliquots of the mineral separates were analyzed.

Hornblende from the pink, medium-grained, equigranular granodiorite of the Zamora batholith (sample 101E; Fig. 1) consists of very slightly chloritized subhedral to euhedral crystals, 2–5 mm in length, and evenly dispersed within the rock. Hornblende (locally slightly chloritized) from a late granodiorite porphyry dike located near the center of the San Carlos prospect (sample 138; Fig. 1) forms 5 to 7 mm-long euhedral crystals dispersed throughout the rock. In both of these cases, hornblende showing minimal chloritization was hand-picked from heavy mineral separates.

Coarse-grained muscovite from the hydrothermal breccia located along the eastern edge of the San Carlos prospect (sample 81; Fig. 1) forms subhedral to euhedral, 0.5–1.5 mm crystals in a quartz matrix with minor chalcopyrite and molybdenite.

Geochronological results

Nambija district

The zircon and titanite ages (Table 1) are presented on concordia diagrams (Fig. 3). The weighted mean $^{206}Pb/^{238}U$ ages (Fig. 3) are used for assessment of their age because the $^{207}Pb/^{235}U$ ages are biased by the uncertainty on the isotopic compositions of corrected blank and common lead.

Table 2 Re–Os data for molybdenite samples from the Nambija and Pangui Cu–Mo–Au districts, Zamora batholith, southeast Ecuador

Sample number	AIRIE run no.	Mine	Re (ppm)	^{187}Os (ppb)	Common Os	Age (Ma)
Nambija district						
DTR437, prospect dump	MDID-191	El Tierrero	2,280.2 (7)	3,488 (1)	2.1±1.2	145.9±0.5
DTR438, prospect dump	MDID-182	El Tierrero	2,550 (4)	3,889 (1)	0.84±0.27	145.5±0.5
DTR438, prospect dump	MDID-192	El Tierrero	2,512.4 (5)	3,835 (1)	2.5±2.2	145.6±0.5
DTR536, surface sample	MDID-526	Guaysimi–David	135.0 (2)	208.0 (9)	0.02±0.02	147.0±0.8
Pangui district						
SC091198, 144.80 m	CT-115	San Carlos	831.6 (9)	1,376 (3)	0.408±0.001	157.8±0.6
SC091198, 144.80 m	CT-135	San Carlos	743.5 (5)	1,224 (2)	11.47±0.09	157.0±0.6
PA020398, 249.5 m	CT-136	Panantza	585.2 (4)	941 (2)	5.88±0.02	153.3±0.5
Sutsu, surface sample	CT-137	Sutsu	1,061.9 (7)	1,725 (3)	0.984±0.002	154.9±0.5

Sample weights ranged from 10 to 30 mg. Initial $^{187}Os/^{188}Os$ for age calculation=0.2±0.1. Ages calculated using $^{187}Os=^{187}Re\ (e^{lt}-1)$ and ^{187}Re decay constant=1.666×10^{-11} year^{-1} (Smoliar et al. 1996). Concentration uncertainties reported at 2σ for last digit indicated; ages at 2σ uncertainty. Reported uncertainties in Re–Os ages include all analytical uncertainties and propagation of the uncertainty in $\lambda^{187}Re$. Blank corrections for Re and ^{187}Os for all samples are insignificant due to high Re. CT samples run by NTIMS using Carius tube dissolution and single Re and Os spikes (Markey et al. 1998). MDID samples run by NTIMS using Carius tube dissolution and Re–double Os spike to correct for common Os and mass fractionation (Markey et al. 2003). For CT runs, carried out in the mid-1990s, blanks for these samples were Re=17 to 18 pg, total Os=6 to 8 pg, $^{187}Os/^{188}Os$=0.5 to 8.3. For MDID runs, blanks vary from Re=1.16±0.03 to 4.5±0.1 pg, total Os=1.9±0.1 to 0.344±0.008 pg, $^{187}Os/^{188}Os$=0.25±0.01 to 0.381±0.023. Measurable common Os in some samples represents minor chalcopyrite or pyrite included with molybdenite separate. Run MDID-115 underspiked for Re and repeated with correct spiking in run MDID-135. Replicate analyses of SC091198 represented by runs CT-115 and CT-135 are from two different mineral separates from the same sample. Replicate analyses of DTR438 represented by runs MDID-182 and MDID-192 are from same mineral separate. Run MDID-525 estimated at 10% molybdenite suggesting true Re concentration for this sample is >1,000 ppm

Zircon data for the two samples (DTR64 and DTR184) of the Fortuna porphyritic quartz–diorite intrusion (Fig. 3a) are in excellent agreement (individual $^{206}Pb/^{238}U$ ages of 145.47 ±0.50 Ma for DTR64 and 145.63±0.19 Ma for DTR184). An identical $^{206}Pb/^{238}U$ age (within error) of 145.47±0.30 Ma was obtained for zircons of the Campanillas–Katy porphyritic granodiorite intrusion (sample DTR69). Therefore, the $^{206}Pb/^{238}U$ ages of zircons from Fortuna and Campanillas–Katy are the same within uncertainty and can be pooled together to yield a combined weighted age of 145.38±0.14 Ma (±0.21 Ma with decay constant error for comparison with Re–Os ages; n=10).

The titanite data (Fig. 3b) exhibit a slight shift to the right of the concordia curve, which could be due to a slightly inaccurate isotopic composition of the common lead used for correction, using the model of Stacey and Kramers (1975) for an age of 145 Ma. Applying the average common Pb isotope compositions measured on nine pyrite samples from the Nambija skarns (Chiaradia et al. 2004) does not result in better concordance. Because we are only considering $^{206}Pb/^{238}U$ ages, such analytical bias is irrelevant. The $^{206}Pb/^{238}U$ mean weighted age for titanites 1 and 2 of sample DTR64 is 145.43±0.33 Ma, which is the same within error as the $^{206}Pb/^{238}U$ mean weighted age of the three titanites of sample DTR184 (145.45±0.29 Ma). Pooling the five titanite dates from the two Fortuna samples yields a mean weighted $^{206}Pb/^{238}U$ age of 145.44±0.15 Ma. Note that from the above calculations, we have excluded titanites 3 and 4 of sample DTR64, which, compared to all other titanites from Fortuna, yielded a significantly older discordant age ($^{206}Pb/^{238}U$ age of 157.6±0.4 Ma) and a slightly younger concordant age ($^{206}Pb/^{238}U$ age of 143.5±0.2 Ma), possibly due to lead loss.

The $^{206}Pb/^{238}U$ mean weighted age of the three hydrothermal titanites from the Campanillas–Katy endoskarn is

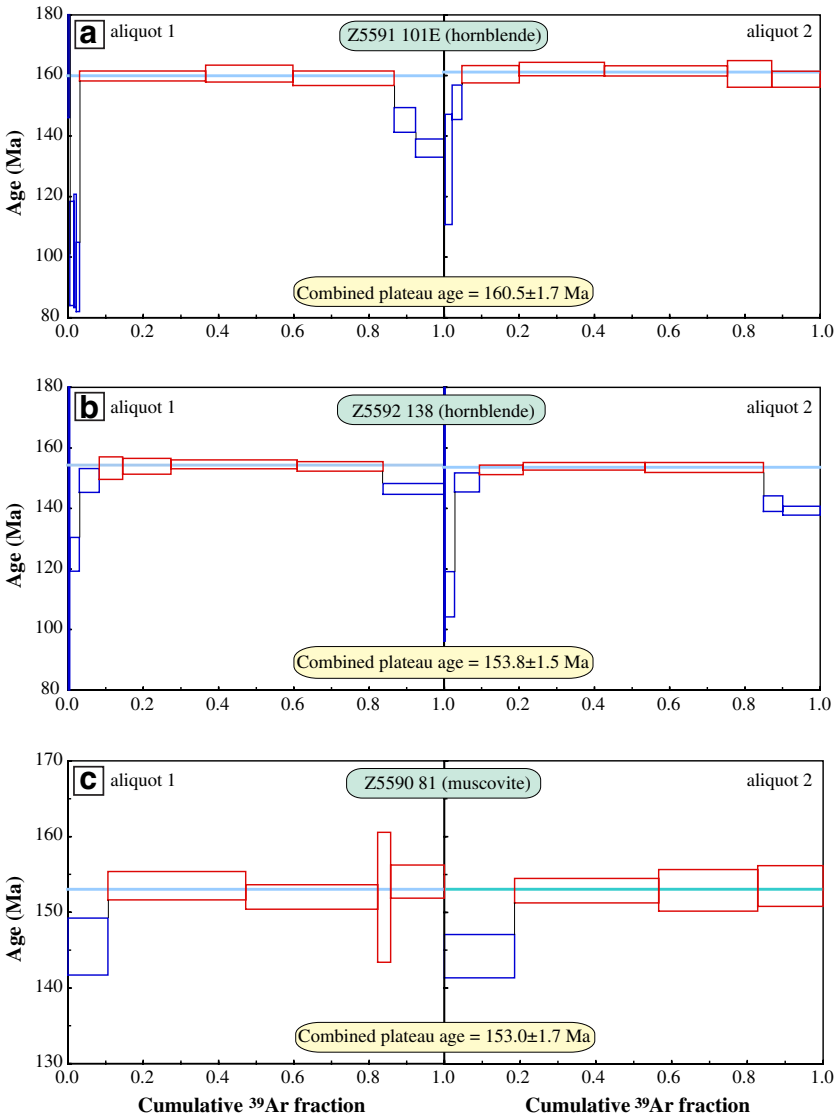

Fig. 4 $^{40}Ar/^{39}Ar$ plateau ages of samples from the San Carlos prospect (Pangui district) obtained from laser step-heating. For each sample, two aliquots have been analyzed. Combined plateau ages of each sample are calculated from the combination of the plateau steps (*red boxes*) of the two aliquots. All plateau ages are reported with 2σ errors including a *J*-factor error of 0.6% (*J*-factor is nominal, referenced to FCT-SAN=28.02 Ma; Renne et al. 1998). *Blue boxes* are rejected steps. Box heights are ±2σ

Table 3 Analytical results of $^{40}Ar/^{39}Ar$ age determinations on minerals from the San Carlos prospect (Pangui district)

Power[a]	Volume $^{39}Ar \times 10^{-11}$ cc	$^{36}Ar/^{39}Ar$	$^{37}Ar/^{39}Ar$	$^{38}Ar/^{39}Ar$	$^{40}Ar/^{39}Ar$	$\%^{40}Ar$ (atm)	$*^{40}Ar/^{39}Ar$	f_{39}[b] (%)	Apparent age[c] (Ma)
81 muscovite; J=0.001970±0.000011 (Z5590)									
2.3	0.4554	0.0139±0.0019	0.001±0.008	0.004±0.011	46.743±1.084	8.8	42.629±1.149	4.9	145.46±3.77
3.0	1.5825	0.0036±0.0006	0.006±0.001	0.005±0.011	46.155±0.563	2.3	45.090±0.577	16.9	153.51±1.88
3.4	1.518	0.0029±0.0009	0.003±0.001	0.003±0.011	45.486±0.425	1.9	44.630±0.497	16.2	152.01±1.62
3.9	0.1478	0.0170±0.0058	0.038±0.010	0.023±0.016	49.646±2.130	10.1	44.618±2.629	1.6	151.97±8.59
12.0	0.6132	0.0094±0.0013	0.006±0.002	0.009±0.011	48.039±0.573	5.8	45.255±0.670	6.6	154.05±2.19
Aliquot 2									
2.3	0.9352	0.0083±0.0010	0.010±0.003	0.005±0.011	44.702±0.861	5.5	42.246±0.869	10	144.21±2.85
3.0	1.9228	0.0037±0.0006	0.004±0.001	0.001±0.011	45.971±0.476	2.4	44.888±0.497	20.5	152.86±1.62
3.4	1.3229	0.0037±0.0008	0.005±0.001	0.001±0.011	46.010±0.822	2.4	44.903±0.841	14.1	152.90±2.75
12.0	0.8669	0.0062±0.0012	0.007±0.001	0.001±0.011	46.901±0.772	3.9	45.078±0.821	9.3	153.47±2.68
101E hornblende; J=0.001967±0.000011 (Z5591)									
Aliquot 1									
2.3	0.0453	3.8934±0.5173	2.055±0.301	2.451±0.342	1232.108±158.658	93.4	81.602±40.017	0.2	268.49±122.41
3.0	0.1086	0.6452±0.0449	1.227±0.087	0.304±0.029	220.007±14.555	86.7	29.345±5.126	0.5	101.22±17.20
3.4	0.0753	0.2657±0.0227	1.410±0.103	0.080±0.021	108.113±7.559	72.6	29.604±5.583	0.3	102.08±18.72
3.9	0.0974	0.1797±0.0114	2.249±0.116	0.176±0.019	80.144±4.147	66.3	27.038±3.399	0.4	93.46±11.45
4.6	3.6864	0.0213±0.0015	8.614±0.052	1.099±0.014	53.398±0.301	11.8	47.105±0.511	15.3	159.82±1.66
5.1	2.548	0.0181±0.0017	8.281±0.116	1.060±0.019	52.694±0.760	10.2	47.339±0.861	10.6	160.58±2.79
5.8	2.9542	0.0106±0.0013	7.348±0.099	1.190±0.021	50.008±0.660	6.3	46.874±0.735	12.3	159.07±2.39
6.8	0.623	0.0214±0.0024	7.080±0.167	1.105±0.037	48.972±1.149	12.9	42.654±1.237	2.6	145.31±4.05
12.0	0.8507	0.0204±0.0026	6.996±0.085	0.874±0.018	45.838±0.529	13.1	39.819±0.911	3.5	136.01±3.00
Aliquot 2									
2.3	0.0457	6.1762±0.5821	2.060±0.195	2.586±0.253	1946.316±178.699	93.8	121.255±41.157	0.2	385.82±117.96
3.9	0.2422	0.5819±0.0264	1.879±0.076	0.347±0.021	209.626±7.094	82	37.674±5.513	1	128.94±18.21
4.3	0.3308	0.1141±0.0053	6.995±0.117	0.673±0.023	78.167±1.284	43.2	44.437±1.746	1.4	151.14±5.70
4.6	1.998	0.0235±0.0016	8.435±0.132	1.146±0.025	54.240±0.857	12.8	47.283±0.876	8.3	160.40±2.84
5.1	2.9739	0.0188±0.0016	9.099±0.096	1.091±0.016	53.361±0.558	10.4	47.805±0.686	12.3	162.09±2.22
5.8	4.297	0.0142±0.0016	8.471±0.049	1.198±0.013	51.822±0.257	8.1	47.624±0.517	17.8	161.51±1.68
6.8	1.5342	0.0269±0.0033	7.657±0.159	1.151±0.028	55.248±1.115	14.4	47.314±1.353	6.4	160.50±4.39
12.0	1.6843	0.0507±0.0019	7.690±0.114	1.032±0.021	61.748±0.806	24.2	46.781±0.811	7	158.77±2.64
138 hornblende; J=0.001964±0.000011 (Z5592)									
Aliquot 1									
2.3	0.0463	2.8191±0.4366	2.497±0.389	1.146±0.182	870.534±133.334	95.7	37.486±21.653	0.2	128.16±71.49
3.9	0.2893	0.2292±0.0064	2.534±0.081	0.194±0.012	104.216±2.143	65	36.482±1.684	1	124.84±5.57
4.3	0.6444	0.0398±0.0022	6.563±0.162	0.670±0.022	55.672±1.302	21.1	43.909±1.210	2.1	149.23±3.95
4.6	0.7398	0.0628±0.0022	5.800±0.134	0.791±0.025	63.726±1.429	29.1	45.163±1.152	2.5	153.32±3.75
5.1	1.5294	0.0159±0.0015	6.438±0.098	0.830±0.022	50.047±0.748	9.4	45.346±0.806	5.1	153.91±2.62
5.8	4.0427	0.0109±0.0011	6.277±0.049	0.871±0.015	48.778±0.346	6.6	45.547±0.458	13.4	154.57±1.49

6.8	2.7311	0.0119±0.0011	6.115±0.053	0.878±0.016	48.853±0.383	7.2	45.341±0.485	9.1	153.90±1.58
12.0	1.9573	0.0180±0.0013	6.297±0.067	0.670±0.014	48.374±0.466	11	43.057±0.556	6.5	146.45±1.82
Aliquot 2									
2.3	0.0659	1.7481±0.1671	1.978±0.171	0.664±0.074	566.775±48.646	91.1	50.224±22.801	0.2	169.71±73.55
3.9	0.4416	0.1894±0.0078	2.223±0.046	0.179±0.012	88.489±1.557	63.3	32.513±2.239	1.5	111.67±7.46
4.3	1.197	0.0290±0.0016	6.056±0.119	0.644±0.021	52.275±1.001	16.4	43.719±0.961	4	148.61±3.14
4.6	2.1082	0.0101±0.0012	6.257±0.059	0.772±0.018	47.990±0.341	6.2	44.993±0.480	7	152.76±1.56
5.1	5.876	0.0075±0.0010	6.101±0.039	0.871±0.012	47.563±0.253	4.7	45.347±0.390	19.5	153.92±1.27
5.8	5.7349	0.0085±0.0012	6.098±0.052	0.846±0.013	47.740±0.376	5.3	45.231±0.501	19	153.54±1.63
6.8	0.9326	0.0143±0.0012	4.241±0.081	0.556±0.017	45.793±0.774	9.2	41.577±0.787	3.1	141.61±2.58
12.0	1.8211	0.0132±0.0011	4.539±0.049	0.573±0.015	44.764±0.359	8.7	40.861±0.453	6	139.26±1.49

[a] As measured by laser in percent of full nominal power (10 W)
[b] Fraction ^{39}Ar as percent of total run
[c] Errors are analytical only and do not reflect error in irradiation parameter J. All uncertainties quoted at 2σ level

145.34±0.19 Ma, which is again indistinguishable within error from the $^{206}Pb/^{238}U$ mean weighted age of the Fortuna titanites (145.44±0.15 Ma). Pooling together all hydrothermal titanites from the two Fortuna samples and the Campanillas–Katy sample (n=8) yields a $^{206}Pb/^{238}U$ mean weighted age of 145.52±0.11 Ma (±0.19 Ma with decay constant error for comparison with Re–Os ages).

Re–Os ages for the Nambija and Pangui molybdenite samples are presented in Table 2 together with Re and Os concentration values. Molybdenites from the two retrograde stage skarn type III vein samples from El Tierrero–Nambija (DTR437 and DTR438), including a replicate analysis of DTR438, yield identical dates of 145.5 Ma within error (Table 2), which, pooled together, yield a mean weighted age of 145.67±0.28 Ma. The molybdenite from the David porphyry Cu–Mo prospect yields a slightly older age of 147.0±0.8 Ma, but additional age data are needed to define a true age difference.

Incorporation of small amounts of chalcopyrite±pyrite was accounted for by measurement and correction for common Os (Table 2). The common Os content for all analyses is insignificant, given the very high Re concentrations (i.e., radiogenic ^{187}Os) obtained for all samples. Re concentrations at the many hundreds to thousands of parts per million level (as in this study) are typically associated with subduction-related porphyry Cu–(Mo–Au) systems globally (Stein et al. 2001, 2004; Zimmerman et al. 2008) and stand in contrast to notably low Re levels in molybdenites of metamorphic origin that may be associated with W–Mo mineralization (Bingen and Stein 2003; Stein 2006; Raith and Stein 2006). The analysis for the David prospect was diluted by about 90% quartz (AIRIE run MDID-526 in Table 2). Therefore, the true Re concentration associated with this molybdenite is about ten times higher than the 135 ppm reported in the data of Table 2. In addition, the fine-grained nature of the molybdenite in samples from the Nambija district means that some silicate dilution is present in all separates and indicates that the true Re concentrations for all samples may be significantly higher than the >2000 ppm reported.

Pangui district

Re–Os ages of molybdenite for three prospects from the Pangui district range from 157.8±0.6 Ma (San Carlos) to 154.9±0.5 Ma (Sutsu) and 153.3±0.5 Ma (Panantza). Two replicates of the San Carlos sample (SC091198) yielded the same age within error (Table 2).

The $^{40}Ar/^{39}Ar$ plateau ages obtained on magmatic and hydrothermal minerals from the samples of the San Carlos prospect vary from 161 Ma (Zamora batholith), through 153 Ma (porphyritic granodiorite dike) to 152 Ma (hydrothermal breccia) (Fig. 4 and Table 3). All aliquots from the three samples investigated yielded plateau ages based on

more than 75% ^{39}Ar released from three to four consecutive steps (Fig. 4). Repeat aliquots from the same sample yielded the same age within error.

Aliquots 1 and 2 of the hornblende from the Zamora batholith (sample 101E) show some Ar loss in the low-temperature steps, which may indicate minor Ar loss from grain margins. Aliquot 1 shows a drop in apparent age in the highest temperature steps (6.8 and 12.0 W; Table 3 and Fig. 4a). This is probably due to degassing of a secondary phase, possibly chlorite. The combined plateau age calculated for the indicated steps in aliquots 1 and 2 is 160.5±1.7 Ma (Fig. 4a). Regressing the most radiogenic steps through the composition of atmospheric argon (^{40}Ar/^{36}Ar=295.5) on an inverse isochron diagram (not shown) results in a date of 160.6±1.6 Ma (MSWD=0.6), which is within error of the plateau age.

Aliquots 1 and 2 of hornblende from the late porphyritic granodiorite dike (sample 138) both show Ar loss in the low-temperature steps. Both aliquots also show a drop in the apparent age in the highest temperature steps (6.8 and 12.0 W; Table 3 and Fig. 4b), which may indicate the degassing of a secondary phase, probably chlorite. The combined plateau age calculated for the indicated steps in aliquots 1 and 2 is 153.8±1.5 Ma (Fig. 4b). Regressing the most radiogenic steps through the composition of atmospheric argon (^{40}Ar/^{36}Ar=295.5) on an inverse isochron diagram (not shown) results in a date of 153.5±1.5 Ma (MSWD=1.8), which is within error of the plateau age.

Aliquots 1 and 2 of coarse-grained muscovite from the San Carlos hydrothermal breccia (sample 81) show slight Ar loss in the first step, but otherwise define good plateaus with a combined plateau age of 153.0±1.7 Ma (Fig. 4c). Regressing the most radiogenic steps through the composition of atmospheric argon (^{40}Ar/^{36}Ar=295.5) on an inverse isochron diagram (not shown) results in a date of 151.9±1.5 Ma (MSWD=0.5), which is again within error of the plateau age.

Discussion

Nambija district

The high-resolution U–Pb geochronologic data presented above demonstrate that, for the Fortuna and Campanillas deposits, there is no resolvable age difference between the crystallization of the endoskarn stage hydrothermal titanite (145.52±0.19 Ma, including decay constant error, n=8) and magmatic zircon (145.38±0.21 Ma, including decay constant error, n=10) of the associated porphyritic stocks. Based on field studies and petrographic–geochemical data, these stocks are genetically related to skarn formation (Fontboté et al. 2004, Markowski et al. 2006).

Indistinguishable ^{206}Pb/^{238}U ages obtained for zircons from Fortuna (145.55±0.14 Ma) and Campanillas–Katy (145.47±0.30 Ma) indicate that porphyritic intrusions were contemporaneous at both sites. Likely, they represent offshoots of a common larger and deeper magmatic chamber.

Re–Os molybdenite ages for two samples from retrograde skarn stage type III veins at Nambija–El Tierrero (145.92±0.46 Ma for sample DTR437 and 145.58±0.45 Ma for sample DTR438) are indistinguishable within 2σ error from U–Pb ages of both magmatic zircons and hydrothermal titanites. Therefore, intrusion of the porphyritic stock and formation of the prograde and retrograde skarn stages at Nambija occurred within a time frame that is not resolvable by our high-resolution Re–Os and U–Pb dates (i.e., less than about 0.7 My; Fig. 5). Because gold deposition predates type III veins of the retrograde skarn stage and postdates hydrothermal titanite of the prograde endoskarn stage, gold deposition is constrained to have occurred at about 145 Ma, "simultaneously" with skarn formation. We conclude that gold mineralization at Nambija is chronologically associated with skarn formation and intrusion of the porphyritic stocks cutting the Zamora batholith and Piuntza unit (Fig. 5). These ages are supported by geological observations and petrographic and geochemical data presented earlier (Fontboté et al. 2004; Markowski et al. 2006).

The wide range of K–Ar ages (Jurassic to Eocene) previously reported by Prodeminca (2000) on K-feldspar and sericite from the Nambija district (Fig. 5) reflects variable degrees of disturbance of the K–Ar system in these samples, most probably related to uplift of the Eastern Cordillera and Subandean zone following the Late Cretaceous accretion of the Pallatanga oceanic terrane onto the South American margin (Spikings et al., 2000; Pratt et al. 2005; Vallejo et al. 2006).

The molybdenite age for porphyry Cu–Mo mineralization at the David prospect (Fig. 1) is marginally older (147.0±0.8 Ma) than skarn formation and gold mineralization (~146–145 Ma), although more data are needed to establish a real age difference between these systems. Nevertheless, it is noteworthy that, whereas the three skarn-related mineralized sites are aligned along the same N–S structural lineament in the northern part of the Nambija district, the David porphyry Cu–Mo prospect (in the central part of the Nambija district), also situated along a N–S structural lineament, is offset about 2 km to the east by a NW-trending fault (Fig. 1). These may, therefore, be two separate magmatic-hydrothermal systems, albeit broadly related to the same regional magmatic–metallogenic event.

Pangui district

Re–Os ages for molybdenites from three prospects (San Carlos, Panantza, and Sutsu) of the Pangui porphyry Cu–

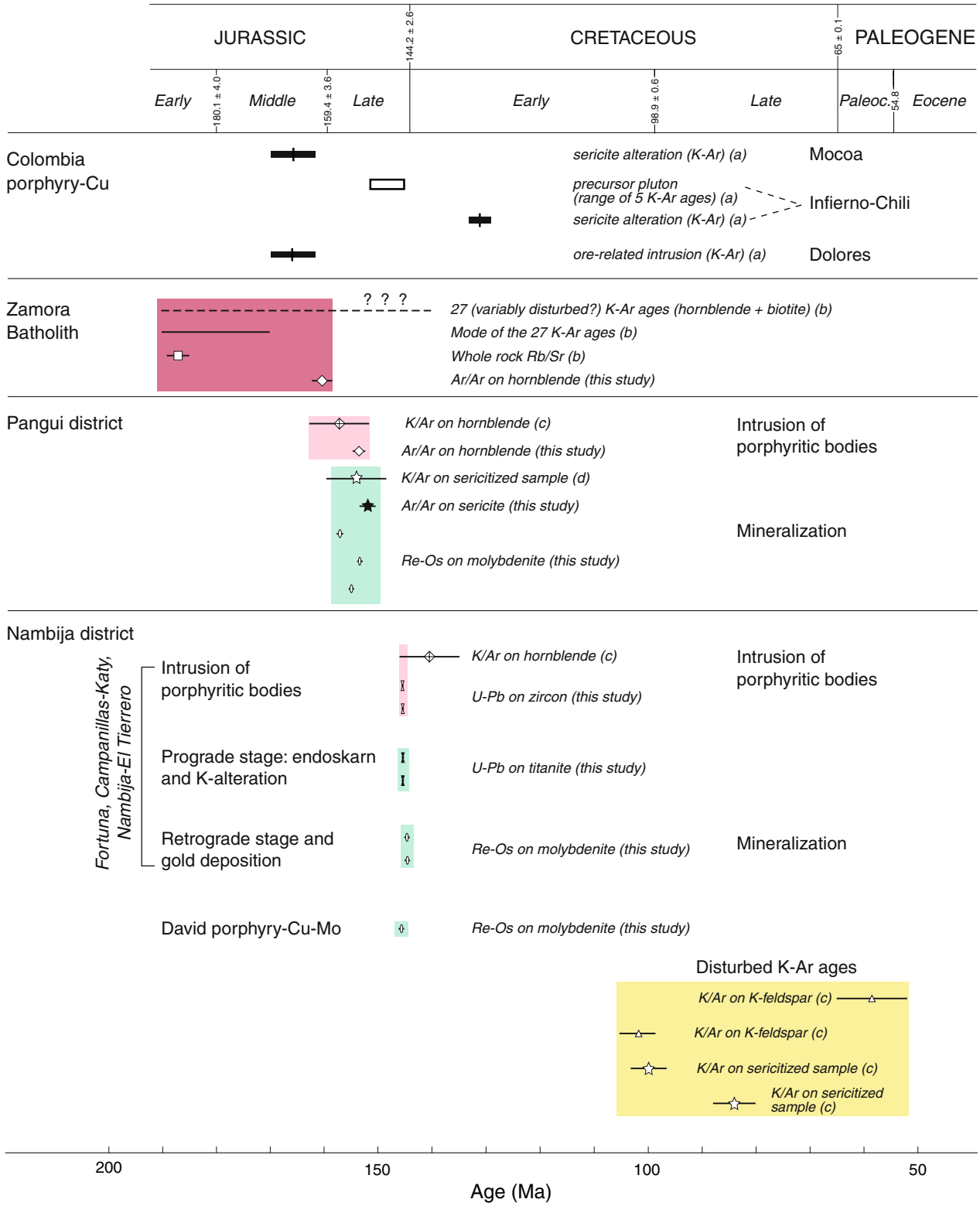

References: (a) Sillitoe (1988) and references therein; (b) Litherland et al. (1994); (c) Prodeminca (2000); (d) Gendall et al. (2000)

Fig. 5 Summary of radiometric ages of magmatic rocks and hydrothermal minerals from the Jurassic metallogenic belt of Colombia and Ecuador (data from this study and from the indicated references). Absolute ages of stage boundaries are from Gradstein et al. (1995) and Berggren et al. (1995)

Mo district suggest episodic mineralization at ~157 Ma (San Carlos), ~155 Ma (Sutsu), and ~153 Ma (Panantza). K–Ar dates (~157 to ~145 Ma) reported by Gendall et al. (2000) exhibit less disturbance than observed for the Nambija area, and the older K–Ar dates overlap the Re–Os age range. A $^{40}Ar/^{39}Ar$ age of 153.0±1.7 Ma for hydrothermal breccia at San Carlos suggests protracted magmatic–hydrothermal activity not only at the district scale, but also at the deposit scale (from ~157 Ma for Re–Os molybdenite to ~153 Ma for the hydrothermal breccia at San Carlos). These dates are similar to the $^{40}Ar/^{39}Ar$ age (153.8±1.5 Ma) of a porphyritic granodiorite dike at San Carlos that cuts the Zamora batholith (160.5±1.7 Ma).

The age comparison between the Nambija and the Pangui district suggests a protracted magmatic–hydrothermal history at Pangui (157–152 Ma) that is 7 to 10 My older than that occurring at Nambija (147–145 Ma). As at Nambija, mineralization is associated with late porphyritic stocks (≥~153 Ma) cutting the Zamora batholith (age ≥160.5 Ma; Fig. 5).

Jurassic metallogeny in Ecuador and the Northern Andes

The existence of a Jurassic porphyry Cu–Mo belt along the western margin of the Northern Andes was proposed by Gendall et al. (2000) following the discovery of such deposits in the Pangui district of Ecuador. This new district represents the southern continuation of the porphyry Cu–Mo belt of Colombia (Sillitoe 1988) and opens up new possibilities for porphyry exploration along the length of this belt. The new Jurassic age for gold mineralization at Nambija and the geochronologic evidence for its genetic association with skarn formation allow us to extend the Jurassic metallogenic belt of the Northern Andes some 100 km to the south of the Pangui district (Fig. 6) and add a new mineralization style (skarn) and a new commodity (gold) to its potential exploration targets. The genetic link between these different mineralization styles is supported not only by their broadly similar ages but also by similar Pb isotopic compositions of ore minerals from the porphyry Cu deposits of Colombia (Sillitoe and Hart 1984) through those of the Pangui area to the skarn and porphyry Cu deposits of the Nambija district (Chiaradia et al. 2004). Lead (and possibly Cu and Au) were derived from a similar reservoir along-strike of this Jurassic arc, most likely identifiable as a homogeneous enriched mantle that had limited interaction with lower crust-type lithologies (Sillitoe and Hart 1984; Chiaradia et al. 2004).

Combining our new age data with the geological and isotopic information given above, we can try to place the Jurassic porphyry-related deposits of the Northern Andes in their geodynamic framework (Fig. 7). Continued subduction during the Jurassic led to the intrusion of large volumes of magmas along the western margin of the Amazon craton between 190 and 160 Ma (e.g., Zamora, Abitagua, and Azafran batholiths in Ecuador) and coeval volcanism (Mishualli Formation), whereas marine to continental rift deposits during the Lower Jurassic and volcaniclastic sediments during the Upper Jurassic were deposited in the

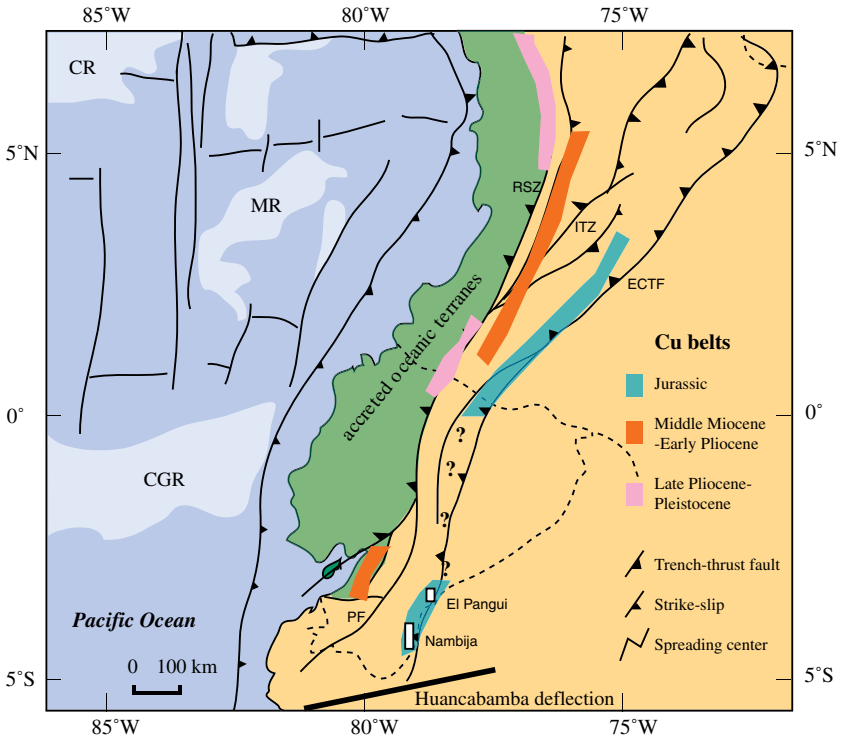

Fig. 6 Metallogenic belts of the Northern Andes, including the Jurassic belt with the new extension into southeastern Ecuador (redrawn from Sillitoe 1988 and Corredor 2003)

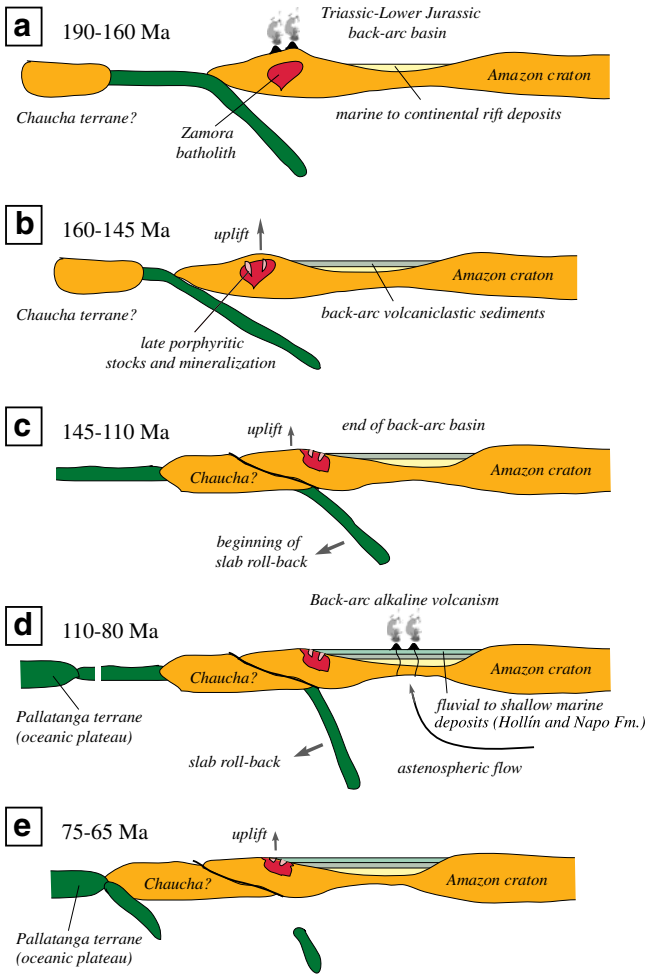

Fig. 7 Cartoons showing the Jurassic to Late Cretaceous evolution of the Ecuadorian continental margin (modified from Barragan et al. 2005 on the basis of geochronologic data of this study and taking into account the Pallatanga accretion ages of Vallejo et al. 2006). *A* 190–160 Ma: subduction-related magmatism (Zamora batholith and Misahualli volcanic sequence) and deposition of marine to continental rift deposits in the back-arc basin. *B* 160–145 Ma: intrusion of the late porphyritic stocks and formation of porphyry-related mineralization during uplift; first stages of collision of the Chaucha terrane (or other mechanism which shut off subduction-related magmatism); end of subduction-related magmatism; deposition of volcaniclastic sediments in the back-arc. *C* 145–110 Ma: collision of the Chaucha terrane (or other mechanism which shut off subduction-related magmatism); sedimentation hiatus and uplift; end of back-arc basin extension. *D* 110–80 Ma: marine transgression (Hollín and Napo Formations) accompanied by slab roll-back and alkaline back-arc volcanism. *E* 75–65 Ma: collision of the oceanic plateau terrane of Pallatanga and uplift

back-arc basin (cartoons A and B in Fig. 7). Shallow level (~4 km depth) porphyritic stocks were intruded into the equigranular Zamora batholith between 157 (San Carlos, Pangui district) and 145 Ma (Nambija district) (cartoon B in Fig. 7). They represented the last intrusive phases of subduction-related magmatism in the Jurassic arc of the Northern Andes (Fig. 5). Although depths of crystallization are not available for the Zamora batholith, the transition from the equigranular texture of the Zamora batholith to the porphyritic texture of the late stocks, intruded at shallow levels (3 to 4 km depth, see above), suggests that intrusion of the late stocks occurred during uplift of the area. Hydrothermal mineralization was coeval with the intrusions of these late shallow level porphyritic stocks and lasted 2 My at Nambija and 5 My at Pangui. This is consistent with the observation that many porphyry-related deposits worldwide form near the end of major periods of magmatism, contraction or transpression, and uplift (Sillitoe 1997; Tosdal and Richards 2001; Richards 2003). Indeed, the definition of Nambija as Jurassic and the recent discovery in the same Cordillera del Cóndor of the high-grade low-sulfidation epithermal Au–Ag Fruta del Norte deposit (Stewart and Leary 2007) show that the Jurassic volcano-plutonic arc of the Northern Andes could well be comparable to the Cenozoic volcanoplutonic arcs of the Central Andes with their rich endowments of porphyry-related and epithermal deposits.

The Jurassic arc-related magmatism ceased perhaps due to the Late Jurassic–Early Cretaceous accretion of allochthonous terranes (cartoon C in Fig. 7) onto the western margin of the Amazon craton. However, other processes, such as slow, oblique, low-angle subduction (e.g., Kennan and Pindell 2003), slab flattening, or changes of plate motions (e.g., Aspden et al. 1987; Jaillard et al. 1990, 2000) cannot be ruled out as possible causes of the cessation of subduction-related magmatism. Cessation of arc magmatism was followed by a several million years long sedimentation hiatus and continued uplift in the area (cartoon C in Fig. 7). Deposition of the transgressive marine Hollín Formation occurred during the Aptian–Albian directly on top of the Zamora batholith and Misahualli volcanic rocks and was accompanied by back-arc alkaline volcanism related to slab roll-back (Barragan et al. 2005; cartoon D in Fig. 7). Accretion of oceanic terranes and renewed uplift of the old Jurassic arc occurred during the Late Cretaceous (cartoon E in Fig. 7), resulting in erosion and exposure of the Jurassic porphyry and skarn deposits.

Conclusions

New high-resolution U–Pb, Re–Os, and $^{40}Ar/^{39}Ar$ ages for magmatic and hydrothermal minerals from skarn and porphyry Cu deposits of the Nambija district and porphyry Cu–Mo prospects of the Pangui district (southeastern Ecuador) have enabled us to place these mineral deposits in their regional geologic and geodynamic contexts.

We show that the gold and porphyry Cu–Mo mineralization at Nambija and Pangui, respectively, is chronologically related to intrusion of porphyritic stocks cutting the Jurassic Zamora batholith and Piuntza unit, and at

Nambija, to skarn formation associated with the emplacement of these bodies. The virtually identical ages (~145 Ma) at Fortuna, Campanillas, and El Tierrero–Nambija for porphyry intrusion and prograde and retrograde skarn formation (which also bracket gold mineralization) indicate that these three sites in the northern part of the Nambija district belong to the same short-lived magmatic–hydrothermal system, which was developed along a N–S structural lineament. A similar-aged magmatic–hydrothermal system (~147 Ma) occurs in the central part of the Nambija district (David porphyry Cu–Mo prospect) and may be related to a distinct porphyry stock emplaced along a parallel but separate N–S structural lineament.

The U–Pb, Re–Os, and $^{40}Ar/^{39}Ar$ ages presented in this study indicate that porphyry-related mineralization in the Nambija and Pangui districts occurred in association with the latest intrusive pulses of a protracted (several tens of million years) subduction-related magmatic event and during uplift, in a similar way to many porphyry-related deposits elsewhere in the world.

The Late Jurassic age for Nambija gold mineralization and porphyry formation at Pangui allows us to extend the Jurassic metallogenic belt of the Northern Andes from Colombia to the Pangui and Nambija areas of southeastern Ecuador. The skarn-related gold mineralization at Nambija also allows us to add a new mineralization style (Au-skarn) to the metallogenic belt associated with the Jurassic volcanoplutonic arc of the Northern Andes.

Acknowledgements We acknowledge the financial support of the Swiss Fonds National to the Geneva Isotope Laboratories. Some of the Re–Os work was supported by the U.S. National Science Foundation (EAR-0087483 to HS), and the mineral separations and isotopic analyses were performed by R. Markey and A. Zimmerman of the AIRIE Program at Colorado State University. The technical assistance of M. Ovtcharova and M. Senn for U–Pb analyses is kindly acknowledged. The financial support of Gencor (later Billiton) to J. Coder, J. Richards, M. Villeneuve, and H. Stein for the work at Pangui is greatly appreciated, and we are particularly grateful for the support and encouragement of G. Koll.

References

Aspden JA, McCourt WJ, Brook M (1987) geometrical control of subduction-related magmatism: the Mesozoic and Cenozoic plutonic history of Western Colombia. J Geol Soc London 144:893–905

Aspden JA, Litherland M (1992) The geology and Mesozoic collisional history of the Cordillera Real, Ecuador. Tectonophysics 205:187–204

Barragan R, Baby P, Duncan R (2005) Cretaceous alkaline intra-plate magmatism in the Ecuadorian Oriente Basin: geochemical, geochronological and tectonic evidence. Earth Planet Sci Lett 236:670–690

Berggren WA, Kent DV, Swisher CC, Aubry MP (1995) A revised Cenozoic geochronology and chronostratigraphy. In: Berggren WA, Kent DV, Swisher CC, Aubry M, Hardenbol J (eds) Geochronology, time scales and global stratigraphic correlation. Society for Sedimentary Geology Special Publication 54:129–212

Bingen B, Stein HJ (2003) Molybdenite Re–Os dating of biotite dehydration melting in the Rogaland high-temperature granulites, S Norway. Earth Planet Sci Lett 208:181–195

Chiaradia M, Fontboté L, Paladines A (2004) Metal sources in mineral deposits and crustal rocks of Ecuador (1°N–4°S): a lead isotope synthesis. Econ Geol 99:1085–1106

Coder JM (2001) Geologic setting, geochronologic relationships and lithogeochemistry of the Pangui porphyry copper district, southeast Ecuador. MSc Thesis, University of Alberta, Edmonton, Canada, p 108

Corredor F (2003) Seismic strain rates and distributed continental deformation in the northern Andes and three-dimensional seismotectonics of northwestern South America. Tectonophysics 372:147–166

Deckart K, Clark AH, Celso AA, Ricardo VR, Bertens AN, Mortensen JK, Fanning M (2005) Magmatic and hydrothermal chronology of the giant Río Blanco porphyry copper deposit, Central Chile: implications of an integrated U–Pb and $^{40}Ar/^{39}Ar$ database. Econ Geol 100:905–934

Fontboté L, Vallance J, Markowski A, Chiaradia M (2004) Oxidized gold skarns in the Nambija District, Ecuador. In: Sillitoe RH, Perello J, Vidal CE (eds) Andean metallogeny: new discoveries, concepts, and updates. Society of Economic Geologists Special Publication 11:341–357

Gemuts I, Lopez G, Jimenez F (1992) Gold deposits of southern Ecuador. SEG Newsletter 11:13–16

Gendall IR, Quevedo LA, Sillitoe RH, Spencer RM, Puente CO, Leon JP, Povedo RR (2000) Discovery of a Jurassic porphyry copper belt, Pangui area, southern Ecuador. SEG Newsletter 43(1):8–15

Gradstein FM, Agterberg FP, Ogg JG, Hardenbol J, Van Veen P, Thierry J, Huang Z (1995) A Triassic, Jurassic, and Cretaceous time scale. In: Berggren WA, Kent DV, Swisher CC, Aubry M, Hardenbol J (eds) Geochronology, time scales and global stratigraphic correlation. Society for Sedimentary Geology Special Publication 54:95–126

Gustafson LB, Hunt JP (1975) The porphyry copper deposit at El Salvador, Chile. Econ Geol 70:857–912

Hughes RA, Pilatasig LF (2002) Cretaceous and Tertiary terrane accretion in the Cordillera Occidental of the Andes of Ecuador. Tectonophysics 345:29–48

Jaillard E, Soler P, Carlier G, Mourier T (1990) Geodynamic evolution of the northern and central Andes during early to middle Mesozoic times: a Tethyan model. J Geol Soc London 147:1009–1022

Jaillard E, Hérail G, Monfret T, Díaz-Martínez E, Baby P, Lavenu A, Dumont JF (2000) Tectonic evolution of the Andes of Ecuador, Peru, Bolivia and northernmost Chile. In: Cordani UG, Milani EJ, Thomaz-Filho A, Campos DA (eds) Tectonic evolution of South America. Publication of the 31st International Geological Congress, Rio de Janeiro, pp 481–559

Jaillard E, Guillier B, Bonnardot MA, Hassani R, Lapierre H, Toro J (2005) Orogenic buildup of the Ecuadorian Andes. In: Sempéré T (ed) 6th International Symposium on Andean Geodynamics (ISAG 2005, Barcelona), extended abstracts, pp 404–407

Kennan L, Pindell J (2003) Terrane accretion in the Northern Andes: the Caribbean connection. Abstract, AAPG International Conference Barcelona, Spain, 21–24 September 2003, paper 83442

Kerr AC, Aspden JA, Tarney J, Pilatasig LF (2002) The nature and provenance of accreted oceanic terranes in western Ecuador: geochemical and tectonic constraints. J Geol Soc London 159:577–594

Litherland M, Aspden JA, Jemielita RA (1994) The metamorphic belts of Ecuador. British Geological Survey Overseas Memoir 11, Keyworth, UK, p 147

Maksaev V, Munizaga F, McWilliams M, Fanning M, Mathur R, Ruiz J, Zentilli M (2004) New chronology for El Teniente, Chilean Andes, from U–Pb, 40Ar/39Ar, Re–Os, and fission–track dating: implications for the evolution of a supergiant porphyry Cu–Mo deposit. In: Sillitoe RH, Perello J, Vidal CE (eds) Andean metallogeny: new discoveries, concepts, and updates. Society of Economic Geologists Special Publication 11:15–54

Markey RJ, Stein HJ, Morgan JW (1998) Highly precise Re–Os dating of molybdenite using alkaline fusion and NTIMS. Talanta 45:935–946

Markey RJ, Hannah JL, Morgan JW, Stein HJ (2003) A double spike for osmium analysis of highly radiogenic samples. Chem Geol 200:395–406

Markowski A (2003) The gold skarn of Fortuna, (Nambija District, Cordillera del Cóndor, Ecuador). MSc Thesis, University of Geneva, Switzerland, p 184. Available at http://www.unige.ch/sciences/terre/mineral/

Markowski A, Vallance J, Chiaradia M, Fontboté L (2006) Mineral Zoning and Gold occurrence in the Fortuna skarn Mine, Nambija district, Ecuador. Miner Deposita 41:301–321

Paladines A, Rosero G (1996) Zonificación mineralogénica del Ecuador. Edición Laser, Quito, p 146

Pratt WT, Duque P, Miguel P (2005) An autochthonous geological model for the eastern Andes of Ecuador. Tectonophysics 399:251–278

Prodeminca (2000) Depositos porfidicos y epi-mesotermales relacionados con intrusiones de la Cordillera del Cóndor: Evaluacion de distritos mineros del Ecuador. UCP Prodeminca Proyecto MEM BIRF 36-55 EC 5, p 223

Quispesivana L (1996) Geología de los cuadrángulos de Puesto Llave y Rió Comaína. Instituto Geológico Minero y Metalúrgico, Lima, Perú, p 120, (64)

Raith JG, Stein HJ (2006) Variscan ore formation and metamorphism at the Felbertal scheelite deposit (Austria): constraining tungsten mineralisation from Re–Os dating of molybdenite. Contrib Mineral Petrol 152:505–521

Renne PR, Swisher CC, Deino AL, Karner DB, Owens TL, DePaolo DJ (1998) Intercalibration of standards, absolute ages and uncertainties in $^{40}Ar/^{39}Ar$ dating. Chem Geol 145:117–152

Richards JP (2000) Lineaments revisited. SEG Newsletter 42(1):14–20

Richards JP (2003) Tectono-magmatic precursors for porphyry Cu–(Mo–Au) deposit formation. Econ Geol 98:1515–1533

Romeuf N, Aguirre L, Soler P, Féraud G, Jaillard E, Ruffet G (1995) Middle Jurassic volcanism in the Northern and Central Andes. Rev Geol Chile 22:245–259

Sillitoe RH (1988) Epochs of intrusion-related copper mineralization in the Andes. J South Am Earth Sci 1:89–108

Sillitoe RH, Hart SR (1984) Lead-isotope signatures of porphyry copper deposits in oceanic and continental settings, Colombian Andes. Geochim Cosmochim Acta 48:2135–2142

Sillitoe RH (1997) Characteristics and controls of the largest porphyry copper–gold and epithermal gold deposits in the circum-Pacific region. Aust J Earth Sci 44:373–388

Smoliar MI, Walker RJ, Morgan JW (1996) Re–Os ages of group IIA, IIIA, IVA and IVB iron meteorites. Science 271:1099–1102

Spikings RA, Seward D, Winkler W, Ruiz GM (2000) Low temperature thermochronology of the northern Cordillera Real, Ecuador: tectonic insights from zircon and apatite fission track analysis. Tectonics 19:649–668

Spikings RA, Winkler W, Seward D, Handler R (2001) Along-strike variations in the thermal and tectonic response of the continental Ecuadorian Andes to the collision with heterogeneous oceanic crust. Earth Planet Sci Lett 186:57–73

Stacey JS, Kramers JD (1975) Approximation of terrestrial lead isotope evolution by a two-stage model. Earth Planet Sci Lett 26:207–221

Stein HJ (2006) Low-rhenium molybdenite by metamorphism in northern Sweden: recognition, genesis, and global implications. Lithos 87:300–327

Stein HJ, Hannah JL, Zimmerman A, Markey R, Sarkar SC, Pal AB (2004) A 2.5 Ga porphyry Cu–Mo–Au deposit at Malanjkhand, central India: implications for Late Archean continental assembly. Precambrian Res 134:189–226

Stein HJ, Markey RJ, Morgan JW, Hannah JL, Schersten A (2001) The remarkable Re–Os chronometer in molybdenite: how and why it works. Terra Nova 13:479–486

Stewart PW, Leary S (2007) The Fruta del Note epithermal Au–Ag deposit, SE Ecuador. In: Andrew CJ et al (eds) Digging deeper. Proceedings of the 9th Biennial SGA Meeting, Dublin, 20–23 August 2007, pp 719–722

Tosdal RM, Richards JP (2001) Magmatic and structural controls on the development of porphyry Cu±Mo±Au deposits. In: Richards JP, Tosdal RM (eds) Structural controls on ore genesis. Rev Econ Geol 14:157–181

Vallance J, Markowski A, Fontboté L, Chiaradia M (2003) Mineralogical and fluid inclusion constraints on the genesis of gold-skarn deposits in the Nambija district (Ecuador). In: Eliopoulos D et al (ed) Mineral exploration and sustainable development. Millipress, Rotterdam, pp 399–402

Vallejo C, Spikings RA, Luzieux L, Winkler W, Chew D, Page L (2006) The early interaction between the Caribbean Plateau and the NW South American Plate. Terra Nova 18:264–269

Zimmerman A, Stein HJ, Hannah JL, Kozelj D, Bogdanov K, Berza T (2008) Tectonic configuration of the Apusini–Banat–Timok–Srednogorie belt, Balkans–South Carpathians, constrained by high precision Re–Os molybdenite ages. Miner Deposita 43:1–21